

Flying Capacitor Converter as a wind turbine interface – modulation and MPPT issues

Abstract. This paper shows an application of three-level Flying Capacitor Converter in an AC-DC-AC system interfacing a wind turbine. Modulation, Maximum Power Point Tracking issues are discussed. Experimental results are shown with conclusions.

Streszczenie. W artykule przedstawiono aplikację trójpoziomowego przekształtnika z kondensatorami o zmiennym potencjale w układzie AC-DC-AC w zastosowaniu do turbiny wiatrowej podłączonej do sieci energetycznej. Omówione zostało zagadnienie modulacji dla przekształtnika oraz śledzenia punktu mocy maksymalnej. Przedstawiono wyniki eksperymentalne wraz z wnioskami. (**Przekształtnik z kondensatorami o zmiennym potencjale w zastosowaniu do turbiny wiatrowej – zagadnienia modulacji i śledzenia punktu mocy maksymalnej.**)

Słowa kluczowe: przekształtniki wielopoziomowe, AC-DC-AC, modulacja, MPPT.

Keywords: multilevel converters, AC-DC-AC, modulation, MPPT.

Abstract

This paper presents an application of the three-level Flying Capacitor Converter (FCC) in an AC-DC-AC (Back to Back - BtB) system interfacing a wind turbine with an asynchronous generator to the grid. The FCC operates as the machine converter (MC) while also three-level Diode Clamped Converter (DCC) is the grid converter (GC). The control is based on Voltage Oriented Control (VOC) and Indirect-Field Oriented Control (IFOC) methods but it also comprises a Space Vector Modulation (SVM) for the FCC, the Maximum Power Point Tracking (MPPT) to increase the effectiveness of power generation and the Power Feed-Forward to improve system stability. Moreover, the reference machine flux control is proposed as the way to reduce magnetization power losses and raise the output power. Experimental results confirm correct operation of the proposed control structure. Additionally, basic comparison of the FCC and DCC converters features are shortly pointed out. And finally a detailed analysis of flying capacitors voltages balancing is proven by experimental results.

Introduction

There are several advantages of multilevel converters in comparison to two-level converters. Considering power electronics systems the most important are decrease of voltage stress of switches and improved harmonic distortion of output voltage. According to an increased interest in renewable sources and development of medium and high-level power generation systems fed by wind turbines, a good solution for these applications are multilevel converters. However, there are some complications related to that, like more complex modulation algorithm or necessity of eventual, additional capacitors voltages balancing.

There have already been several publications introducing the Diode Clamped Converter (DCC) back-to-back (BtB) system interfacing a wind turbine, for example [1], [2]. This kind of application brings specific conditions for the modulation strategy. With the use of MPPT the wind speed usually keep the modulation index value in the range where zero-voltage vectors content is comparatively high. For the DCC topology only internal transistors of each leg are used to generate the level zero of phase voltage [3][4]. It leads to an unevenness of conduction losses between the leg switches. For this issue the FCC topology brings the solution, which are the redundant states, described in the further section. They require the use of all leg switches. Thanks to that the conduction losses are distributed more evenly.

According to above this paper presents a hybrid multilevel system with a Flying Capacitor Converter (FCC) on the machine side (MS) and DCC on the grid side (GS). The main features of both converters are listed in Table 1 [3][4][7][10]. It presents a short comparison of the modulation complexity and topologies. The hybrid BtB topology has been proposed to confirm a stable operation of the system in wide speed range and voltage range. This BtB converter is connected to the laboratory wind turbine model consisted of an induction generator with DC machine (prime mover) fed by reversible rectifier.

Classical Space Vector Modulation (SVM) was used for both converters, but for DCC it has been already widely described in the literature [3], [4], [7] and here will be omitted. According to that, in section I the Classical SVM algorithm for three phase, three-level FCC is described [9],[10]. The section also includes an overview of problems connected with the implementation. Incorrect flying capacitors (FCs) voltages balancing leads to wrong output voltage levels generation, while undesired switching states can cause high overvoltage. The solutions are presented here. It is of course possible to enhance the classical modulation for multilevel converters, using techniques discussed in [5], [6], [8], [10], [11], [12], [13].

Further sections are dedicated to machine control and DC-link voltage control. In section II a block scheme and short description of IFOC is presented.

Proper work of the system is dependent on fast and correct control of the DC-link voltage. To improve control response dynamic, an active Power Feed-Forward (PFF) is used. It cooperates with the grid side converter control. Section III includes more details and a block scheme of PFF.

For the best exploitation of wind potential for power generation it is necessary to use the Maximum Power-Point Tracking (MPPT). According to that an incremental MPPT algorithm was implemented in the simulation and laboratory model. The results of its performance are presented in section IV. Additional output power can be brought by the machine power losses reduction, obtained with the reference flux control. For this issue the results are also presented.

Laboratory setup is described in section V, while simulation and experimental results for PFF and MPPT implementation are presented in sections VI. Finally section VII contains conclusions.

Table 1. Comparison of the DCC and FCC main features

Feature	DCC	FCC
Elements	1. Additional Clamping-Diodes per each leg 2. DC-link capacitors	1. Additional Flying Capacitor per each leg
Measurement	1. DC-link capacitors voltages 2. phase currents	1. DC-link voltage 2. FCs voltages 3. phase currents
Redundant vectors selecting reliance – Classical SVM	1. DC-link capacitors voltage levels 2. all phase currents signs 3. dependent on all legs state	1. DC-link voltage 2. FC voltage 3. phase current 4. (independent for all legs), all adjacent vectors used in a period
Overmodulation	1. Difficulties with DC-link capacitors voltages balancing, possible instability	1. No problems with FCs voltages balancing, possible higher ripples
Six-Step Mode	1. Both DC-link Capacitors in use simultaneously, no problems with balancing	1. Impossible FCs voltages balancing

For a better overview, the whole system block scheme is presented in figure 1. For control algorithm implementation a dSpace DS1005 card was used.

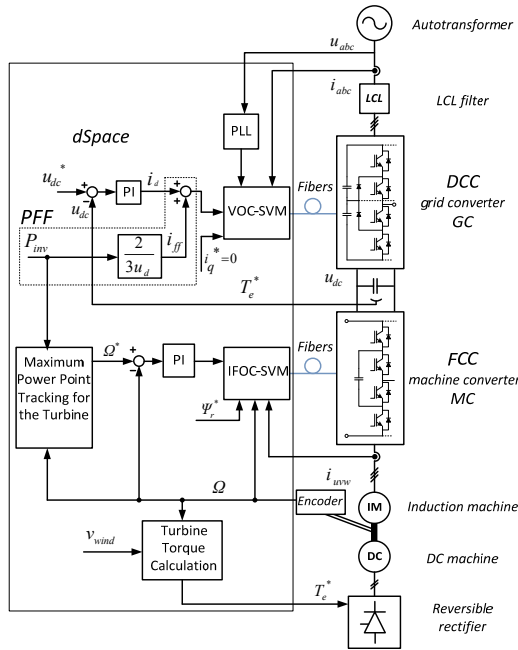


Fig. 1. Complete scheme of AC-DC-AC (BiB) system with control blocks including PFF and MPPT.

Space Vector Modulation In FCC

Each leg of FCC consists of four switches and one Flying Capacitor C_{FCx} (see fig. 1 - [5],[14]) where x refers to leg (phase) a , b or c .

As far as the FCC load is assumed to be symmetric, the Clarke transformation of voltage vectors from natural into stationary $\alpha\beta\gamma$ coordinate system is used with γ equal 0. It's given by:

$$(1) \quad \begin{bmatrix} U_\alpha \\ U_\beta \end{bmatrix} = \begin{bmatrix} 1 & -0.5 & -0.5 \\ 0 & \frac{\sqrt{3}}{3} & -\frac{\sqrt{3}}{3} \end{bmatrix} \begin{bmatrix} U_a \\ U_b \\ U_c \end{bmatrix}$$

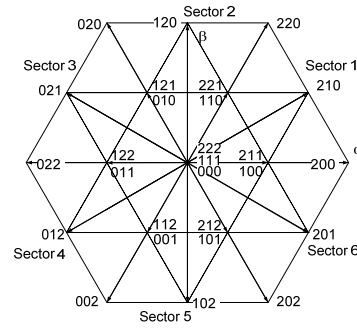


Fig. 2. The voltage $\alpha\beta$ plane for three-level three-phase converter.

Figure 2 shows graphic representation of the Space Vector $\alpha\beta$ voltage plane with possible output voltage vectors of the three-level converter. All voltage vectors are described by three numbers, where the first corresponds to switching states in leg a , the second in leg b and the third in leg c .

Table II presents all possible switching states for single inverter leg and respective generated pole voltage U_x levels (U_x to DC minus). Typically, the FC voltage should equals to half of the DC-link voltage (U_{DC}). With this condition switching state 1 can be divided into two redundant states A and B, which generates the same output voltage $U_x = U_{DC}/2$. Those states are used for independent control of FCs voltages U_{FCx} , one for each sampling period and leg. Table III shows selection between redundant states A or B based on the stator current i_{sx} sign.

Table II Switching States For The Three-Level FCC Leg.

States	T_{ix1}	T_{ix2}	U_x
0	OFF	OFF	0
A	ON	OFF	$U_{DC} - U_{FCx}$
B	OFF	ON	U_{FCx}
2	ON	ON	U_{DC}

Table III Redundant Switching State Selection

Voltage conditions	$i_{sx} < 0$	$i_{sx} > 0$
$U_{FCx} < U_{DC}/2$	B	A
$U_{FCx} > U_{DC}/2$	A	B

For the three-phase three-level FCC the twenty seven voltage states (vectors) can be specified: 3 zero vectors, 12 internal, small amplitude vectors, 6 medium amplitude vectors and 6 external, large amplitude vectors. External vectors divide the plane into six sectors (see fig. 2) and each sector is divided into four triangular regions. Figure 3 presents a detailed view of sector 1. The reference Space Vector \mathbf{U}_{ref} angle θ is used to determine the Space Vector sector location. To calculate duty cycles T_v (where v relates to vector number) of switching states (vectors) it is necessary to define the region number, thus also the modulation coefficient M_{inv} , given by (2) and additional indexes m_1 , m_2 . These indexes are projection of Space Vector on the sector sides, limited by vectors (see fig 3) and according to trigonometric relations are computed with (3). Table IV ([10]) shows D_v calculation methodology which is analogical for all sectors.

$$(2) \quad M_{inv} = \frac{U_{ref} \cdot \pi}{U_{DC}}$$

$$(3) \quad m_1 = M_{inv} \left(\cos \Theta - \frac{\sin \Theta}{\sqrt{3}} \right), \quad m_2 = 2M_{inv} \frac{\sin \Theta}{\sqrt{3}}$$

Table IV. Region Number And Vectors Durations Calculation.

Modulation index	Region	Duty cycle
$m_1 > 1$	1	$D_{v1}=m_1-1; D_{v2}=m_2; D_{v4}=2-m_1-m_2$
$m_1 \leq 1; m_2 \leq 1; m_1+m_2 > 1$	2	$D_{v4}=1-m_2; D_{v5}=1-m_1; D_{v2}=m_1+m_2-1$
$m_2 > 1$	3	$D_{v2}=m_1+m_2-1; D_{v3}=m_2-1; D_{v5}=2-m_1-m_2$
$m_1 \leq 1; m_2 \leq 1; m_1+m_2 \leq 1$	4	$D_{v4}=m_1; D_{v5}=m_2; D_{v0}=1-m_1-m_2$

It must be noted that delay between computations and hardware realization has significant impact on FCs voltages balancing through the PWM modulator, which is based on actual measured values. This may duplicate voltage ripples.

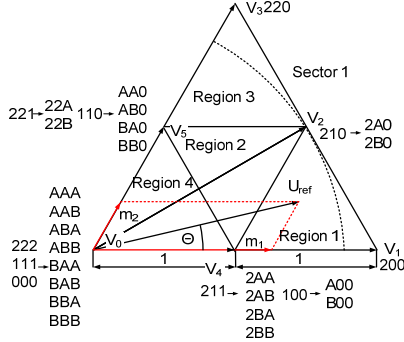


Fig. 3 Sector 1 with division into four regions and possible switching states.

Therefore, to compensate the delay effect, the estimation of the FCs voltages at the end of the subsequent sampling period was introduced with the equation:

$$(1) \quad U_{FCx}(t+1) = U_{FCx}(t) + \frac{i_{sx}(t+0.5)dT_{sx}}{C_{FC}}$$

where $U_{FCx}(t)$ is the measured FC_x voltage, dT_{sx} is duration of the pulse influencing the FC_x voltage and $i_{sx}(t+0.5)$ is the estimated amplitude of measured $i_{sx}(t)$ phase current in the middle of sampling period:

$$(2) \quad i_{sx}(t+0.5) = i_{sx}(t) + \frac{i_{sx}(t) - i_{sx}(t-1)}{0.5T_s}$$

Using $U_{FCx}(t+1)$ value it is possible to eliminate the delay and choose the appropriate A or B state.

	$\frac{V_4}{2}$	V_1	V_2	$\frac{V_4}{2}$	$\frac{V_4}{2}$	V_2	V_1	$\frac{V_4}{2}$		$\frac{V_4}{2}$	V_1	V_2	$\frac{V_4}{2}$	$\frac{V_4}{2}$	V_2	V_1	$\frac{V_4}{2}$
$T_{i_{a1}}$	1A	2	2	2	2	2	2	1A	$T_{i_{a1}}$	1B	2	2	2	2	2	2	1B
$T_{i_{a2}}$									$T_{i_{a2}}$								
$T_{i_{b1}}$	0	0	1A	1A	1A	1A	0	0	$T_{i_{b1}}$	0	0	1B	1B	1B	1B	0	0
$T_{i_{b2}}$									$T_{i_{b2}}$								
$T_{i_{c1}}$	0	0	0	1A	1A	0	0	0	$T_{i_{c1}}$	0	0	0	1B	1B	0	0	0
$T_{i_{c2}}$									$T_{i_{c2}}$								

Fig. 4 Duty cycle for region 1 for chosen state A-(a) and B-(b) of sector 1.

Finally, when duty cycles are set, the signals can be generated. Figure 4 illustrates switching pattern sample for the region 1 of sector 1 (see fig. 3). As it can be noticed, all adjacent vectors are included in modulation. Figure 3a) presents generated signals for the case when state A is used, while figure 3b) for state B.

Moreover, FCs voltages balancing leads to necessity of switching between state A and B in subsequent periods which, in the worst case occurs at the end of the first and the beginning of the second (fig. 5 (a)). In that case all the four signals are changing, which can cause overvoltage. To eliminate this phenomenon and provide better switching distribution between particular switches a modification of the switching pattern, presented in figure 5(b) was introduced. Using that, both objectives can be reached.

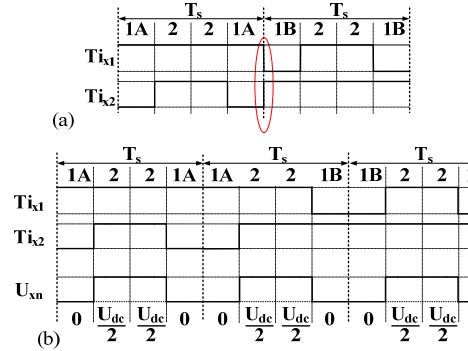


Fig. 5 Transition between state A and B: (a) classical pattern, (b) modified pattern.

Indirect Field-Oriented Control – General Information

Fig. 6 shows a block scheme of IFOC which was implemented in the system. It has been widely described in the literature [15], [16]. Reference stator currents in rotating coordinates dq are calculated using reference rotor flux ψ_r^* module and torque T_e^* , obtained with speed controller. Currents errors are delivered to PI controllers which gives reference voltage in dq coordinates. Thus, after transformation to $\alpha\beta$, PWM signals are generated through SVM.

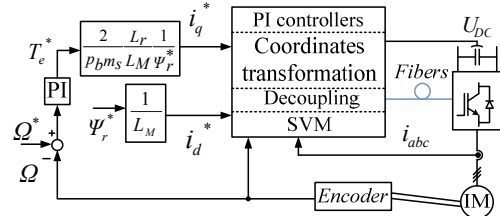


Fig. 6 Block scheme of Indirect Field-Oriented Control (IFOC).

Power Feed-Forward

Power Feed-Forward brings a significant improvement in DC-link voltage control. Considering large step changes of the load, the single PI controller, like in VOC, may not be fast enough to bring the best response and reliability of control. Figure 7 presents a scheme of implemented PFF.

As can be seen, machine power is calculated with:

$$(3) \quad P_{inv} = 1,5(U_{ref\alpha}i_{s\alpha} + U_{ref\beta}i_{s\beta})$$

where P_{inv} is a machine active power, $U_{ref\alpha}$, $U_{ref\beta}$ and $i_{s\alpha}$, $i_{s\beta}$ are reference voltage and stator currents vectors in stationary coordinates.

In the next step correction value i_{ff} is computed with:

$$(4) \quad i_{ff} = \frac{2}{3U_d}$$

where U_d is a part of the grid voltage in rotating coordinates dq. Eventually, the i_{ff} is added to I_{d_ref} part of reference current in rotating coordinates.

The power filter (see fig. 7 [15], [19]) has a significant influence on quality of the feed-forward, hence its time

constant has to be chosen in order to achieve a good dynamic. Thus, to eliminate possible distortions influencing the calculated machine power, the filter cut-off frequency was set to 150Hz. All results will be showed in section V.

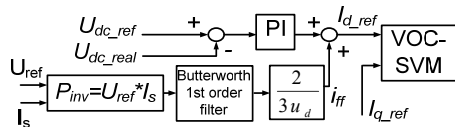


Fig. 7 Block scheme of implemented Power Feed-Forward.

Incremental MPPT For Wind Turbine Generator

Incremental MPPT is based on turbine speed measure and calculation of generated power [17], [18], [19]. Using those values it changes the reference speed with defined step $\Delta\omega$. No additional parameters like turbine characteristic, air density or instantaneous wind speed are necessary. Relative change of generated power is computed in every MPPT period, which means that in each cycle actual power is compared with its value calculated in the previous cycle. Thus, it can be written:

$$(5) \quad P = \left(\frac{P_{actual}}{P_{previous}} \right) - 1$$

The rest of the algorithm will run if ΔP exceeds the required minimal value. The second parameter is the change of reference speed in the last period ($\Delta\omega_{ref1}$) and two periods before the actual one ($\Delta\omega_{ref2}$). Once the ΔP condition is met the tracking algorithm runs. It will change the reference speed with a step $\Delta\omega$ depending on the following conditions:

- If $\Delta P > 0$ (increase of power in last period) and $\Delta\omega_{ref1} \geq 0$ (increase of reference speed in last period), then increase the reference speed (note that the maximum speed must be set),
- If $\Delta P > 0$ and $\Delta\omega_{ref1} < 0$, then continue decreasing the reference speed,
- If $\Delta P < 0$ and $\Delta\omega_{ref2} > 0$ and $\Delta\omega_{ref1} < 0$, then no reference speed change increases generated power; decrease the reference speed with double step $\Delta\omega$,
- If $\Delta P < 0$ and $\Delta\omega_{ref1} \geq 0$, then decrease the reference speed (note that the minimum speed must be set),
- If $\Delta P < 0$ and $\Delta\omega_{ref1} < 0$, then increase the reference speed.

Another method to increase the generated power is based on machine field losses reduction [16][20][21]. When the turbine torque is not nominal, then respective decrease of the reference flux amplitude will have an effect of magnetization losses minimization. The research results are presented in section VII.

Laboratory Setup

The control algorithm was implemented on laboratory setup based on Modular DSP dSPACE DS1005 PPC Board [10], [22], which is the core of dSPACE modular hardware. Experimental setup was connected to the grid by autotransformer. As has been mentioned, the wind turbine was modeled with DC-machine fed by a reversible rectifier (prime-mover) shaft connected with an asynchronous machine. Parameters of AC machine are shown in table 5. The reference torque of the turbine is given by dSPACE calculation, based on the turbine characteristic presented in figure 8.

The whole laboratory setup consisted of:

- Three-level 15kVA DCC/ three-level 3kVA FCC,
- LCL grid filter 2.8mH/6uF/2.2mH,
- 3kW asynchronous machine/ 3kW DC-machine,

- Reversible rectifier,
- dSPACE modular hardware,
- Computer with dSPACE DS1005 and encoder card,
- Tektronix 3034B oscilloscope.

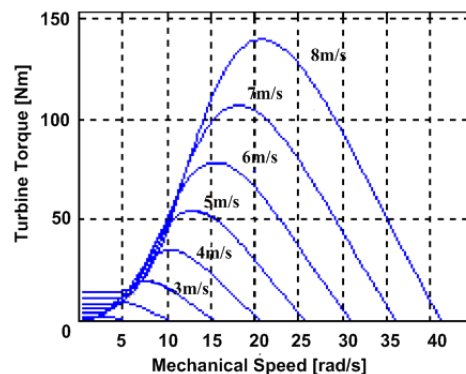


Fig. 8 Mechanical torque characteristic of 3kW turbine. Dependency between angular speed (horizontal axe), turbine torque (vertical axe) and wind speed.

Table 5. Asynchronous Machine Parameters

Parameter	Unit	Value
Nominal power P_n	kW	3
Nominal phase-phase voltage U_{ff}	V	380
Nominal frequency f_n	Hz	50
Stator resistance R_s	Ω	1.84
Stator inductance L_s	H	0.17
Rotor resistance R_r	Ω	1.84
Rotor inductance L_r	H	0.17
Mutual inductance L_M	H	0.16
Inertia J	$kg \cdot m^2$	0.007
Pole pairs p_b		2

Experimental Results

Simulation and experimental research have been investigated for 600V of the DC-link voltage. They gave very similar results, thus only experimental results will be presented.

Flying Capacitor voltage balancing is shown in figure 9 and figure 10. It presents the comparison of modulation algorithm performance for the case when FCs voltage prediction is turned off (fig. 9a and fig. 10a) and turned on (fig. 9b and fig. 10b)). There are two cases of the reference speed, 50rad/s (fig. 9 – only 4th regions operation) and 120rad/s (fig. 10 – 1st, 2nd and 3rd regions operation). It can be seen that FCs voltage prediction results in significant improvement of FCs voltage balancing (about 50% reduction).

Dynamic test of MPPT, relied on generation of wind speed as a trapezoidal wave function (fig. 11). Results were obtained for machine speed controlled by MPPT. Figure 11 presents relation of generated active power (a) and grid phase current (b) to wind speed changes. It can be seen how the algorithm tracks the maximum of generated power. The generator speeds up and slows down accordingly to the wind speed increases or decreases respectively (see the ramp). When the wind speed is constant then it reaches the steady state.

Field losses reduction test result is presented in figure 12. It shows a comparison of the system performance for the reference rotor flux amplitude set to 1Web (fig. 12a) and 0.6Web (fig. 12b). The other conditions, in both cases, were, the same (DC link voltage 300V, wind speed 5.5m/s). As is shown, achieved losses reduction, brought an increase of generated power (in this particular, case almost 50%).

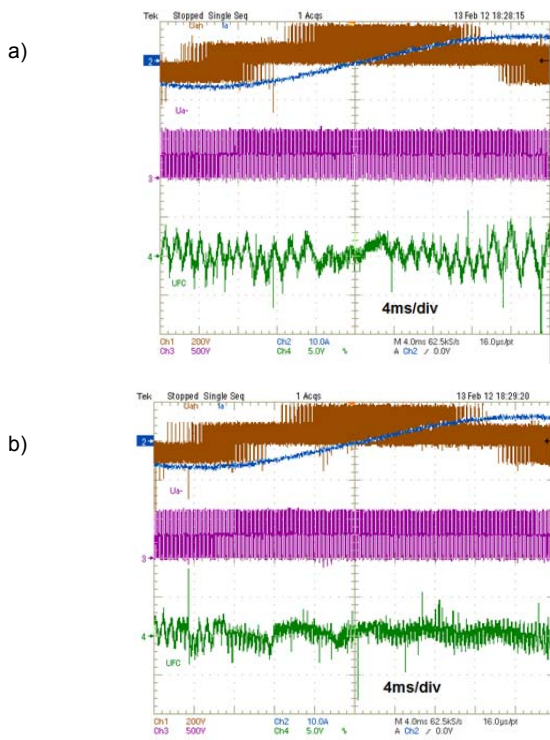


Fig. 9 Balancing of leg A Flying Capacitor voltage; the reference speed – 50rad/s; FCs voltage prediction turned off (a) and turned on (b); from the top: phase voltage (brown) 500[V/div], machine phase current (blue) [10A/div], phase pole voltage [500V/div], FC voltage [5V/div offset 300V].

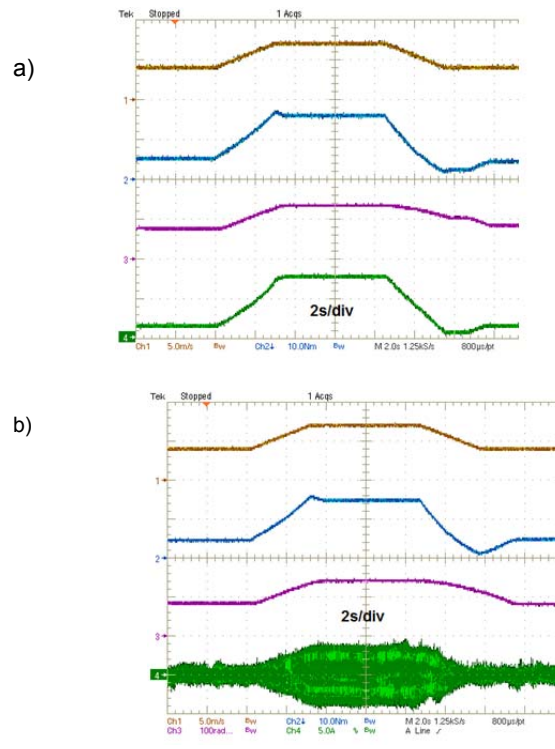


Fig. 11 Trapezoidal wind speed changes (4-7m/s, period 20s); from the top: wind speed [5m/s/div], turbine torque [10Nm/div], reference machine angular speed [100rad/s/div], generated machine power [1kW/div] (a), grid phase current [A] (b).

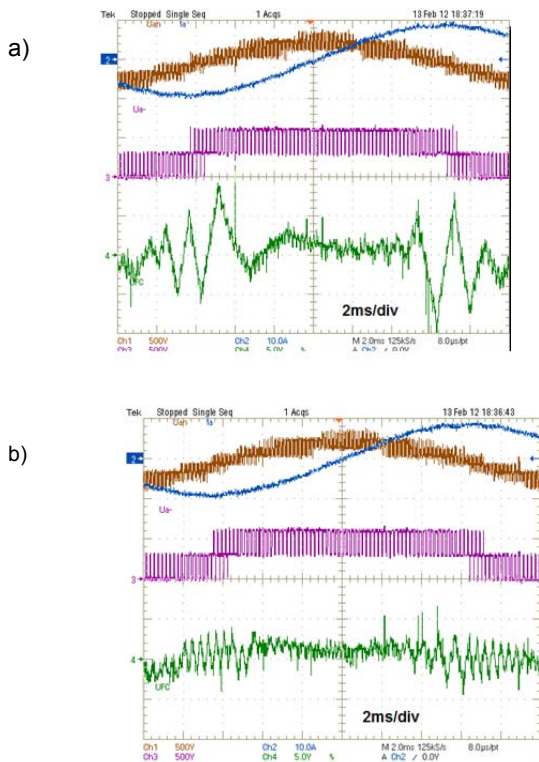


Fig. 10 Balancing of leg A Flying Capacitor voltage; the reference speed – 120rad/s; FCs voltage prediction turned off (a) and turned on (b); from the top: phase voltage (brown) 500[V/div], machine phase current (blue) [10A/div], phase pole voltage [500V/div], FC voltage [5V/div offset 300V].

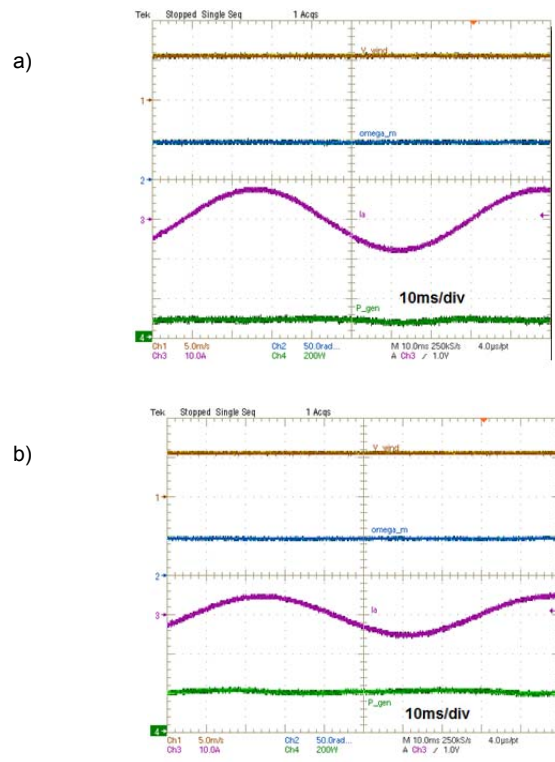


Fig. 12 Steady state operation (constant wind speed – 5.5m/s) with MPPT and the reference rotor flux 1Web - a), and 0.6Web - b); from the top: wind speed [5m/s/div], reference machine angular speed [50rad/s/div], machine phase current [10A/div], generated machine power [200W/div]

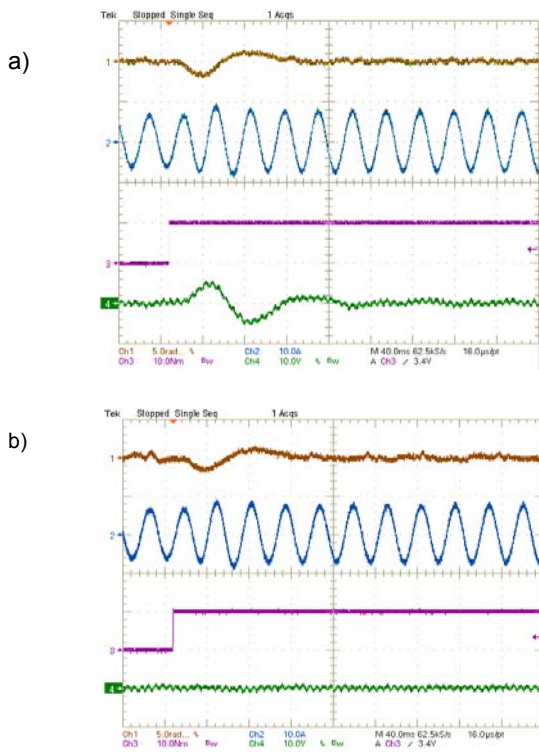


Fig. 13 Step change of load torque 0-10Nm: without PFF (a), with PFF (b); from the top: machine angular speed [5rad/s/div offset 100rad/s], machine (FCC) phase current [10A/div], load torque [10Nm/div], DC-link voltage [10V/div offset 600V].

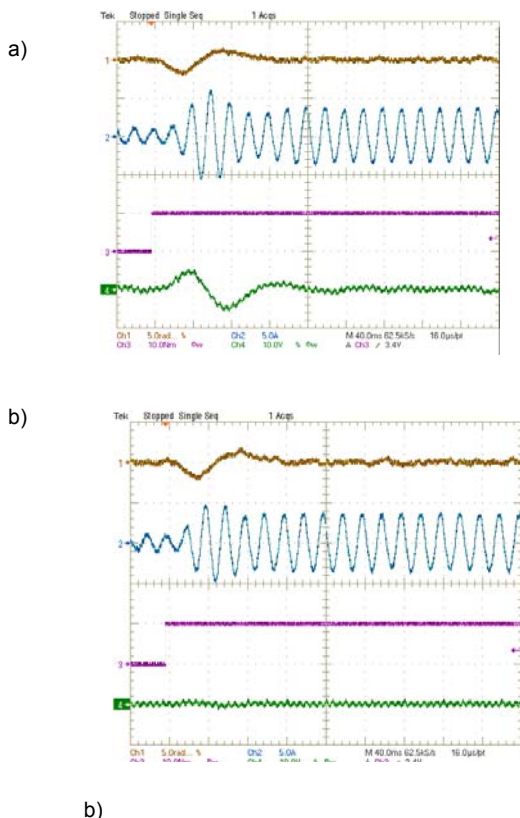


Fig. 14 Step change of load torque 0-10Nm: without PFF (a), with PFF (b); from the top: machine angular speed [5rad/s/div offset 100rad/s], grid (DCC) phase current [5A/div], load torque [10Nm/div], DC-link voltage [10V/div offset 600V].

Figure 13 and 14 present system response to load step change from 0 to 10Nm under the condition of PFF being

turned off (a) and turned on (b). As can be noticed in fig. 13b) and fig. 14b) the DC link voltage remains steady, independently on the load change. Note that in figure 13 machine phase current is shown, while in figure 14 grid phase current. Tests were taken with $U_{DC}=600V$.

Summary and Conclusions

Typical application of the Flying Capacitor Converter (FCC) is an active filter, where the Carrier-Based PWM technique is used for each leg. Considering the machine converter MC in proposed hybrid BtB system, it is preferable to adapt the SVM, thus a standard machine control like FOC or DTC-SVM can be simply used as well as the other presented algorithms.

The Classical SVM for the FCC brings an relatively easy way to control the converter. As it was mentioned in the introduction, the redundant states assure more balanced conduction losses distribution. For this specific application it reduces the stress on the inner switches in comparison to the DCC topology.

However the modulation provides a correct Flying Capacitors (FCs) voltages balancing, in figure 9 and figure 10 it can be seen how high distortions can occur. Using the prediction algorithm, eliminating the delays, had increased the stability of FC voltage. Moreover, the proposed modified switching pattern allows to avoid possible overvoltage, enhancing converter protection.

To achieve a high efficiency of modeled wind turbine power generator, the MPPT algorithm was implemented. Presented results (fig. 10, fig. 11), shows that the Incremental MPPT assures a very good machine reference speed control in reference to the generated power maximum and the actual wind speed in the dynamic and steady states. Moreover, the field losses reduction test, showed that it's possible to increase the efficiency of power generation for a low turbine torque values.

The Power Feed-Forward (PFF) algorithm improved the dynamic of the control response to the load step changes. As shown in figure 13 and figure 14 it has almost no influence on the DC link voltage stability what, as the result, provides a good phase voltages levels generation.

Acknowledgment

This work has been supported by Polish Ministry of Science and Higher Education grant no N N510 331637 in 2009-2011 as scientific project."

REFERENCES

- [1] Bueno E. J., Cobreces S., F. J. Rodriguez, Hernandez A., Espinosa F., Design of a Back-to-Back NPC Converter Interface for Wind Turbines With Squirrel-Cage Induction Generator, *IEEE Transaction on Energy Conversion*, 23 (2008), No. 3, 932-945
- [2] Bueno E., Cobreces S., Rodriguez F., Hernandez A., Espinosa F., Mateos R., et al., Optimized design of a back-to-back NPC converter to be used as interface for renewable energies, *Industrial Electronics Society, IECON 2005. 31st Annual Conference of IEEE*, 2543-2548
- [3] Nabae A., Takahashi I., Akagi H., A New Neutral-Point-Clamped PWM Inverter, *IEEE Transaction on Industrial Applications*, (1981)
- [4] Rodriguez J., Pontt J., Lezana P., Kouro S., Tutorial on Multilevel Converters, *International Conference on Power Electronics and Intelligent Control for Energy Conservation. Warsaw (2005)*
- [5] Meynard T. A., Foch H., Multilevel Conversion: High Voltage Choppers and Voltage-Source Inverters, *IEEE Power Electronics Specialist Conference*, (1992), 397-403
- [6] McGrath B. P., Holmes D. G., Lipo T., Optimized space vector switching sequences for multilevel inverters, *IEEE Transactions on Power Electronics*, (2003), 1293-1301

- [7] Kolomyjski W., Modulation strategies for three-level pwm converter-fed induction machine drive, *Ph.D. dissertation* Warsaw: Warsaw University of Technology (2009)
- [8] McGrath B. P., Holmes D. G., Meynard T., Reduced PWM harmonic distortion for multilevel inverters operating over a wide modulation range, *IEEE Transactions on Power Electronics*, 21 (2006), No. 4, 941-948
- [9] Mendes M. A. S., Peixoto Z. M. A., Seixas P. F., Donoso-Garcia P., A space vector pwm method for three-level flying-capacitor inverters, in *Proc. of IEEE PESC 2001*, 182-187
- [10] Stynski S., Analysis and Control of Multilevel AC-DC-AC Flying Capacitor Converter Fed from Single-Phase Grid, *Ph.D. dissertation*, Warsaw University of Technology (2011)
- [11] Jwu-Sheng H.; Keng-Yuan C.; Te-Yang S.; Chi-Him T., Analytical Solutions of Multilevel Space-Vector PWM for Multiphase Voltage Source Inverters, *IEEE Transactions on Power Electronics*, 26 (2011), No. 5, 1489-1502
- [12] Leon J.I., Vazquez S., Sanchez J.A., Portillo R., Franquelo L.G., Carrasco J.M., Dominguez E. T., Conventional Space-Vector Modulation Techniques Versus the Single-Phase Modulator for Multilevel Converters, *IEEE Trans. on Industrial Electronics*, 57 (2010), No. 7, 2473-2482
- [13] Choi Sanghun, Saeedifard M., A Space Vector Modulation approach for capacitor voltage balancing of Flying Capacitor Converters, Applied Power Electronics Conference and Exposition (APEC), 2011 Twenty-Sixth Annual IEEE (2011), 1174-1179
- [14] Watkins S. J., Zhang L., Multilevel space vector pwm control schemes for a flying-capacitor inverter, in *Proc. of PEMID 2004*
- [15] Jasinski M., Direct power and torque control of AC/DC/AC converter-fed induction motor drives, *PhD. Thesis*, Warsaw University of Technology (2005)
- [16] Kazmierkowski M. P., Control in Power Electronics - Selected Problems (2002)
- [17] Koutroulis E., Kalaitzakis K., Design of a Maximum Power Tracking System for Wind-Energy-Conversion Applications, *IEEE Transactions on Industrial Electronics*, 53 (2006), No. 2, 486-494
- [18] Malinowski M., Stynski S., Control of 3-Level PWM Converter Applied to Variable-Speed Type Turbines, *IEEE Trans. On Ind. Electronics*, 56 (2009), No. 1, 69-77
- [19] Miller A., Muljadi E., Zinger D. S., A variable speed wind turbine power control, *IEEE Transactions on Energy Conversion* (1997), 181-186
- [20] Zengcai Q., Ranta M., Hinkkanen M., Luomi J., et. al., Loss-minimizing flux level control of induction motor drives, *Electric Machines & Drives Conference, IEEE International* (2011)
- [21] Farasat M., Karaman E., et. al., Efficiency-optimized hybrid field oriented and direct torque control of induction motor drive, *Electrical Machines and Systems (ICEMS), International Conference* (2011)
- [22] dSpace GmbH. DS1005 PPC Board, Features, Release 6.5. (2009), Retrieved from www.dspace.com
- Autorzy:** Kamil Antoniewicz, antoniek@ee.pw.edu.pl, (+48 22) 234 5127;
Dr. Marek Jasiński, mja@isep.pw.edu.pl, (+48 22) 234 7675;
Dr. Sebastian Styński, stynskis@isep.pw.edu.pl; (+48 22) 234 7675;
Warsaw University of Technology, Department of Electrical Engineering
Institute of Control and Industrial Electronics
ul. Koszykowa 75a 00-662 Warsaw